General Disclaimer

One or more of the Following Statements may affect this Document

- This document has been reproduced from the best copy furnished by the organizational source. It is being released in the interest of making available as much information as possible.

- This document may contain data, which exceeds the sheet parameters. It was furnished in this condition by the organizational source and is the best copy available.

- This document may contain tone-on-tone or color graphs, charts and/or pictures, which have been reproduced in black and white.

- This document is paginated as submitted by the original source.

- Portions of this document are not fully legible due to the historical nature of some of the material. However, it is the best reproduction available from the original submission.

NASA

Technical Memorandum 85082

APPLICATION OF THE LIENARD-WIECHERT SOLUTION TO A LIGHTNING RETURN STROKE MODEL

Robert Meneghini

August 1983

National Aeronautics and
Space Administration

Goddard Space Flight Center
Greenbelt, Maryland 20771

TM 85082

APPLICATION OF THE LIENARD-WIECHERT SOLUTION TO A LIGHTNING RETURN STROKE MODEL

Robert Meneghini

August 1983

GODDARD SPACE FLIGHT CENTER
Greenbelt, Maryland 20771

ABSTRACT

The electric and magnetic fields associated with the lightning return stroke are expressed as a convolution of the current waveform shape and the fields generated by a moving charge of amplitude one (i.e., the Lienard-Wiechert solution for a unit charge). The representation can be used to compute the fields produced by a current waveform of non-uniform velocity that propagates along a filament of arbitrary, but finite, curvature. To study numerically the effects of linear charge acceleration and channel curvature two simple channel models are used: the linear and the hyperbolic.

APPLICATION OF THE LIENARD-WIECHERT SOLUTION TO A LIGHTNING RETURN STROKE MODEL

by Robert Meneghini

INTRODUCTION

The purpose of the paper is to provide an alternative description of the lightning return stroke and the electric and magnetic fields associated with it. The point of view adopted is that the charge and current densities can be expressed as a collection of moving and stationary charged particles, where the position (and therefore the velocity and acceleration) of each is assumed to be given as a function of time. For the lightning return stroke, charge and current distributions of this kind result in fields that can be interpreted as the fields produced by a moving charge of amplitude one (i.e, the Lienard-Wiechert field solution), multiplied by the current waveform and integrated over what might be termed an effective delay time. For typical return stroke parameters, the sources of the radiation are shown to depend primarily on the channel curvature and the rapid acceleration of charges near the ends of the channel. Since the formulation can be used to analyze channels of arbitrary, but finite, curvature and non-uniform current waveform velocities, it appears to be somewhat more general than either the moment [Hill, 1968, 1969; Marney and Shanmugam, 1971] or the piece-wise linear [LeVine and Meneghini, 1978a, 1978b] field representation.

The organization of the paper is as follows. First, the charge and current densities are expressed in terms of a collection of discrete charged particles. By a limiting process, continuous versions of these sources are obtained from which the scalar and vector potentials and the fields are derived. To complete the solution, the return stroke is modeled simply as a transfer of charge between two points [Uman et al., 1975]. The boundary conditions appropriate to this model then determine the fields. The radiation portion of the fields can be integrated in the case of a finite linear filament if certain restrictions are placed on the velocity of the charges. Although the results are derived in an approximate manner, they compare well with previous work and serve as a guide to the integral representation for the field as the appropriate limit is approached.

In the final section of the paper, numerical results are presented for the electric field as functions of the waveform velocity and the channel curvature. For this purpose two channel geometries are used: the linear and the hyperbolic.

Fields Produced by Charge Motion Along a Filament

The charge density, ρ, and current density, j, associated with a particle of charge Q_o can be described by the equations [Jones, 1964]

$$\rho(\mathbf{x}', t) = Q_o\, \delta(\mathbf{x}' - \mathbf{f}(t))$$

$$\mathbf{j}(\mathbf{x}', t) = Q_o \mathbf{f}'(t)\, \delta(\mathbf{x}' - \mathbf{f}(t))$$

where δ is the Dirac delta function, $\mathbf{x}'$ is an arbitrary position vector and $\mathbf{f}(t)$, $\mathbf{f}'(t)$ are, respectively, the location and velocity of the charge as a function of the time t. For a collection of n+1 charges $(Q_o, \ldots, Q_n)$ where the position of the (j+1)th particle at time T is the same as the position of the jth particle at time $T - \Delta\tau$, the charge and current densities become

$$\rho(\mathbf{x}', t) = \sum_{j=0}^{n} Q_j\, \delta(\mathbf{x}' - \mathbf{f}(t - j\Delta\tau)) \tag{1}$$

$$\mathbf{j}(\mathbf{x}', t) = \sum_{j=0}^{n} Q_j\, \mathbf{f}'(t - j\Delta\tau)\, \delta(\mathbf{x}' - \mathbf{f}(t - j\Delta\tau)) \tag{2}$$

Dividing and multiplying each term of (1) and (2) by $\Delta\tau$ and letting $n \to \infty$, $\Delta\tau \to 0$ and $Q_j \to 0$ in such a way that $Q_j/\Delta\tau$ is finite, then

$$\rho(\mathbf{x}', t) = \int \iota(\tau)\, \delta(\mathbf{x}' - \mathbf{f}(t - \tau))\, d\tau \tag{3}$$

$$\mathbf{j}(\mathbf{x}', t) = \int \iota(\tau)\, \mathbf{f}'(t - \tau)\, \delta(\mathbf{x}' - \mathbf{f}(t - \tau))\, d\tau \tag{4}$$

where ι has units of amperes and is defined by

$$\iota(\tau) = \lim_{\substack{\Delta\tau \to 0 \\ Q_j \to 0}} Q_j/\Delta\tau \tag{5}$$

The electric $\mathbf{E}$ and magnetic $\mathbf{H}$ fields that result from the sources ρ and j can be determined by means of the potentials ϕ and $\mathbf{A}$, where

$$\mathbf{E} = -\nabla\phi - \partial\mathbf{A}/\partial t \tag{6}$$

$$\mathbf{H} = \frac{1}{\mu_o} \nabla \times \mathbf{A} \tag{7}$$

with

$$4\pi\epsilon_0\phi(\mathbf{x}, t) = \int_{\mathbf{x}'}\int_{t'} \frac{\rho(\mathbf{x}', t')}{r}\, \delta(t' - (t - r/c))\, dt'\, d\mathbf{x}' \tag{8}$$

$$4\pi\epsilon_0 c^2\, \mathbf{A}(\mathbf{x}, t) = \int_{\mathbf{x}'}\int_{t'} \frac{\mathbf{j}(\mathbf{x}', t')}{r}\, \delta(t' - (t - r/c))\, dt'd\mathbf{x}' \tag{9}$$

The integrals in (8) and (9) extend over all space and time. The quantity r is the distance from the source point, $\mathbf{x}'$, to the observer, $\mathbf{x}$. Substituting (3) and (4) into (8) and (9) yields

$$4\pi\epsilon_0\phi(\mathbf{x}, t) = \int_{\mathbf{x}'}\int_{t'}\int_{\tau} \frac{\iota(\tau)\, \delta(\mathbf{x}' - \mathbf{f}(t' - \tau))\, \delta(t' - (t - r/c))}{r}\, d\tau dt' d\mathbf{x}' \tag{10}$$

$$4\pi\epsilon_0 c^2\mathbf{A}(\mathbf{x}, t) = \int_{\mathbf{x}'}\int_{t'}\int_{\tau} \frac{\iota(\tau)\mathbf{f}'(t' - \tau)\, \delta(\mathbf{x}' - \mathbf{f}(t' - \tau))\, \delta(t' - (t - r/c))}{r} d\tau\, dt' d\mathbf{x}' \tag{11}$$

In these and the following equations the limits on τ and t' are taken to be $(-\infty, \infty)$. To complete the solution, the boundary conditions are then imposed on the fields themselves.

Assuming that the orders of integration in (10) and (11) can be interchanged, the volume integral can be done directly, giving [Jackson, 1962]

$$4\pi\epsilon_0\phi(\mathbf{x}, t) = \int_{\tau}\int_{t'} \frac{\iota(\tau)\, \delta(t' - (t - r/c))}{r}\, dt'\, d\tau \tag{12}$$

$$4\pi\epsilon_0 c^2\mathbf{A}(\mathbf{x}, t) = \int_{\tau}\int_{t'} \frac{\iota(\tau)\, \mathbf{f}'(t' - \tau)\, \delta(t' - (t - r/c))}{r}\, dt'\, d\tau \tag{13}$$

where

$$r = |\mathbf{x} - \mathbf{x}'| \tag{14}$$

with

$$\mathbf{x}' = \mathbf{f}(t' - \tau)\,. \tag{15}$$

Substituting (12) and (13) into (6) and (7) and carrying out the differentiations yields (Appendix)

$$\mathbf{E}(\mathbf{x}, t) = \frac{1}{4\pi\epsilon_0} \int_{\tau} \iota(\tau)\, (\mathbf{F}_1 + \mathbf{F}_2)\, d\tau \tag{16}$$

and

$$H(x, t) = \frac{1}{4\pi} \int_{\tau} i(\tau) \hat{r} \times (F_1 + F_2)\, d\tau \tag{17}$$

where

$$F_1 = (\hat{r} - v/c)\,(1 - (v/c)^2)/p^3 r^2 \tag{18}$$

$$F_2 = \hat{r} \times ((\hat{r} - v/c) \times v')\,/p^3 c^2 r \tag{19}$$

The distance r and the corresponding unit vector $\hat{r}$ are given by

$$r = |x - x'| \tag{20}$$

$$\hat{r} = (x - x')/r \tag{21}$$

with

$$x' = f(t - |x - x'|/c - \tau) \tag{22}$$

In addition, the velocity v, the acceleration v', and the quantity p are

$$v = f'(t - r/c - \tau) \tag{23}$$

$$v' = f''(t - r/c - \tau) \tag{24}$$

$$p = 1 - v \cdot \hat{r}/c \tag{25}$$

where the prime(s) on f denote differentiation with respect to the argument $u = t - v/c - \tau$.

To compute the fields from (16) and (17) for a given observer x and time t, the integration is performed over all τ. Since the functional form of f is known and if we assume that it is single valued and defined for all values of its argument then at each τ a corresponding value of x' can be found from (22). This immediately yields r; the velocity and acceleration are then obtained from (23) and (24).

To complete the solution for the fields, the following boundary conditions are imposed:

$$f(u) = x'_b \qquad u \leq 0 \tag{26}$$

$$f(u) = x'_t \qquad u \geq t_m \tag{27}$$

$$v(u) = 0 \qquad u \leq 0 \text{ and } u \geq t_m \tag{28}$$

$$v'(u) = 0 \qquad u \leq 0 \text{ and } u \geq t_m \tag{29}$$

and

$$\iota(u) = 0 \qquad u \leq 0 \tag{30}$$

$$\iota(u) \to 0 \qquad u \to \infty \tag{31}$$

where x'_b , x'_t are the distances from the origin to the "bottom" and "top" of the channel and

$$u = t - r/c - \tau \tag{32}$$

To apply these boundary conditions, we use equations (22) and (26) which imply that whenever $\tau \geq t - r/c$, then $x' = x'_b$. But this, in turn, gives $r = |x - x'_b| \equiv r_b$, which is the distance from the bottom of the channel to the observer. Therefore we conclude that if $\tau \geq t - r_b/c$ then $x' = x'_b$. From this relationship and (28) and (29) it follows that $v(t - r_b/c - \tau) = v'(t - r_b/c - \tau) = 0$ when $\tau \geq t - r_b/c$.

Similarly, equations (22) and (27) imply that $x' = x'_t$ when $\tau \leq t - t_m - r_t/c$, where $r_t = |x - x'_t|$ is the distance from the top of the channel to the observer. This condition and (28) and (29) give $v(t - r_t/c - \tau) = v'(t - r_t/c - \tau) = 0$ for $0 \leq \tau \leq t - t_m - r_t/c$.

At those values of τ for which the velocity and acceleration are zero, the integrands of (16) and (17) simplify considerably. Explicitly,

$$F_1 + F_2 = \hat{r}_b/r_b^2 \qquad \tau \geq t - r_b/c \geq 0$$

$$F_1 + F_2 = \hat{r}_t/r_t^2 \qquad 0 \leq \tau \leq t - t_m - r_t/c$$

Therefore, the fields can be written in the form

$$E(x, t) = \frac{1}{4\pi\epsilon_o} \left\{ \int_{\tau_1}^{\tau_2} \iota(\tau)\,(F_1 + F_2)\,d\tau + \hat{r}_b Q_b(t - r_b/c)/r_b^2 + \hat{r}_t Q_t(t - t_m - r_t/c)/r_t^2 \right\} \tag{33}$$

$$H(x, t) = \frac{c}{4\pi} \int_{\tau_1}^{\tau_2} \iota(\tau)\,\hat{r} \times (F_1 + F_2)\,d\tau \tag{34}$$

where

$$\tau_1 = \max(0, t - t_m - r_t/c) \tag{35}$$

$$\tau_2 = \max(0, t - r_b/c) \tag{36}$$

$$Q_b\,(t - r_b/c) = \int_{\tau_2}^{\infty} i(\tau)\,d\tau \tag{37}$$

$$Q_t(t - t_m - r_t/c) = \int_{0}^{\tau_1} i(\tau)\,d\tau \tag{38}$$

with

$$r_b = |\mathbf{x} - \mathbf{x}'_b| \;\; ; \;\; \hat{r}_b = (\mathbf{x} - \mathbf{x}'_b)/r_b \tag{39}$$

$$r_t = |\mathbf{x} - \mathbf{x}'_t| \;\; ; \;\; \hat{r}_t = (\mathbf{x} - \mathbf{x}'_t)/r_t \tag{40}$$

The model of the return stroke implied by the boundary conditions and the sources given in (3) and (4) is simply the transfer of charge from the point $\mathbf{x}'_b$ to the point $\mathbf{x}'_t$ [Uman et al., 1975]. In particular, for times less than r_b/c the observer measures a static electric field arising from a point charge of magnitude $Q_b(0)$ a distance r_b away, where $Q_b(0)$ is the total charge of the system. From the perspective of the observer, and for times greater than r_b/c, charge is extracted from the channel end and begins to propagate along the filament. For times exceeding $t_m + r_t/c$, charge accumulates at the channel top with a magnitude given by (38). As time tends to infinity the entire charge of the system becomes concentrated at the top end point of the channel and the observer measures a static electric field given by $\hat{r}_t Q_t(\infty)/r_t^2$, where $Q_t(\infty) = Q_b(0)$.

Models of this kind have been used in a number of studies [Uman et al., 1975; McLain and Uman, 1977]. Modifications of the model have been discussed by Price and Pierce (1977) and Lin et al. (1980). Despite deficiencies, the model appears adequate for gaining insight into the induction and radiation portions of the field and their dependence on observer location, channel structure, and the shape of the current waveform. Equations (33) and (34) are free space field solutions. To account for the presence of a perfectly conducting ground plane at z = 0, the following image contributions are added to (33) and (34) respectively, to give the total field:

$$\mathbf{E}_I(\mathbf{x},t) = -\frac{1}{4\pi\varepsilon_o}\left\{\int_{\tau_1}^{\tau_2} i(\tau)(\tilde{\mathbf{F}}_1 + \tilde{\mathbf{F}}_2)\,d\tau + \hat{r}_{Ib}Q_b(t - r'_{Ib}/c)/r_{Ib}^2 + \hat{r}_{It}Q_t(t - t_m - r_{It}/c)/r_{It}^2\right\} \tag{41}$$

$$H_I(x, t) = -\frac{c}{4\pi} \int_{\tau_1}^{\tau_2} \iota(\tau)\, \hat{r}_I \times (\tilde{F}_1 + \tilde{F}_2)d\tau \tag{42}$$

The vectors $\tilde{F}_1$, $\tilde{F}_2$ can be defined by (18) and (19) if $\hat{r}$, r, v and v' are replaced by $\hat{r}_I$, r_I, v_I, and v'_I respectively, where

$$r_I = |x - x'_I| \; ; \; \hat{r}_I = (x - x'_I)/r_I \tag{43}$$

$$x'_I = (I - 2\hat{z}\hat{z}) \cdot f(t - r/c - \tau) \tag{44}$$

$$v_I = (I - 2\hat{z}\hat{z}) \cdot f'(t - r/c - \tau) \tag{45}$$

$$v'_I = (I - 2\hat{z}\hat{z}) \cdot f''(t - r/c - \tau) \tag{46}$$

with

$$I = \hat{x}\hat{x} + \hat{y}\hat{y} + \hat{z}\hat{z} \tag{47}$$

the unit vectors $\hat{r}_{Ib}$, $\hat{r}_{It}$ are directed from the "bottom" and "top" of the image filament toward the observer, i.e.,

$$\hat{r}_{Ib} = (x - x'_{Ib})/|x - x'_{Ib}| \tag{48}$$

$$\hat{r}_{It} = (x - x'_{It})/|x - x'_{It}| \tag{49}$$

where $x'_{Ib} = x'_b - 2\hat{z}z$, $x'_{It} = x'_t - 2\hat{z}z$.

In the numerical calculations to be presented, the observer is taken to be at the surface of perfectly conducting ground plane. The total fields (actual plus image) are therefore

$$E_t(x, t) = 2\hat{z}\hat{z} \cdot E(x, t) \tag{50}$$

$$H_t(x, t) = 2(I - \hat{z}\hat{z}) \cdot H(x, t) \tag{51}$$

where the fields on the right hand side of these equations are given by (33) and (34).

Special Cases

There exist several cases for which the integrals in (33) and (34) can be evaluated. To obtain the Lienard-Wiechert solution for a single charge that moves along the path f(t), the current is written as $\iota(\tau) = Q\,\delta(\tau)$. Equations (33) and (34) can be integrated to give

$$4\pi\epsilon_o\,\mathbf{E}(\mathbf{x},t) = \begin{cases} Q\,\hat{\mathbf{r}}_b/r_b^2 & t < r_b/c \\ Q\,(\mathbf{F}_1 + \mathbf{F}_2) & r_b/c < t < t_m + r_t/c \\ Q\,\hat{\mathbf{r}}_t/r_t^2 & t > t_m + r_t/c \end{cases} \tag{52}$$

and

$$\frac{4\pi}{c}\,\mathbf{H}(\mathbf{x},t) = \begin{cases} Q\,\hat{\mathbf{r}}\times(\mathbf{F}_1 + \mathbf{F}_2) & r_b/c < t < t_m + r_t/c \\ 0 & \text{Otherwise} \end{cases} \tag{53}$$

where $\mathbf{F}_1$ and $\mathbf{F}_2$ are given by (18) and (19) if in (20) through (25) τ is set to zero. For example, the r appearing in $\mathbf{F}_1$, $\mathbf{F}_2$ and (53) is given by

$$r = |\mathbf{x} - \mathbf{x}'|$$

where

$$\mathbf{x}' = \mathbf{f}(t - |\mathbf{x} - \mathbf{x}'|/c)$$

Since the velocity and acceleration of the charges are assumed to be zero at the ends of the filament and continuous everywhere, the fields are continuous as well. Equations (52) and (53) are the Lienard-Wiechert field solutions for a charge, initially stationary with respect to the observer, which traverses a finite distance before again coming to rest.

To investigate the behavior of the radiation fields (i.e. the portion of the **E** and **H** field associated with the net power out of a volume enclosing the sources), we obtain from (33) and (34)

$$\mathbf{E}_{rad} = \frac{1}{4\pi\epsilon_o c^2}\int_{\tau_1}^{\tau_2} \frac{\iota(\tau)\,\mathbf{h}}{p^3 r}\,d\tau \tag{54}$$

$$\mathbf{H}_{rad} = \frac{1}{4\pi c}\int_{\tau_1}^{\tau_2} \frac{\iota(\tau)\,\hat{\mathbf{r}}\times\mathbf{h}}{p^3 r}\,d\tau \tag{55}$$

with

$$\mathbf{h} = \hat{\mathbf{r}} \times \left\{ (\hat{\mathbf{r}} - \mathbf{v}/c) \times \mathbf{v}' \right\} \tag{56}$$

For the purpose of identifying the sources of the radiated field it is convenient to express **h** in terms of the channel curvature and arc length. The velocity and acceleration can be written in the forms [Hay, 1953; Stoker, 1969]

$$\mathbf{v}(u) = s' \hat{j}_1 \tag{57}$$

$$\mathbf{v}'(u) = s'' \hat{j}_1 + K s'^2 \hat{j}_2 \tag{58}$$

where s is the arc length along the filament and $s' = ds/du$, $s'' = d^2s/du^2$ where $u = t - r/c - \tau$. The unit vectors $\hat{j}_1$, $\hat{j}_2$ and $\hat{j}_3$ are the tangent vector, principal normal and binormal to the filament, respectively, and form a right-handed orthonormal basis; the quantity K is the curvature.

Substituing (57) and (58) into (56) gives

$$\mathbf{h} = K s' \left\{ \hat{\mathbf{r}} \times [(\hat{\mathbf{r}} \times \hat{j}_2) - s' \hat{j}_3/c] \right\} + s''(\hat{\mathbf{r}} \times (\hat{\mathbf{r}} \times \hat{j}_1)) \tag{59}$$

As in the case of a single charge, two sources of the radiation field can be distinguished [Panofsky and Phillips, 1962; Jones, 1964]. If the speed of the charges is a constant v_o, then $s' = v_o$ and $s'' = 0$ so that

$$\mathbf{h} = K v_o^2 \left\{ \hat{\mathbf{r}} \times [(\hat{\mathbf{r}} \times \hat{j}_2) - (v_o/c) \hat{j}_3] \right\} \tag{60}$$

i.e. the integrands of (54) and (55) are proportional to the channel curvature. On the other hand, if the channel is linear, then $K = 0$ and

$$\mathbf{h} = s'' \hat{\mathbf{r}} \times (\hat{\mathbf{r}} \times \hat{j}_1) \tag{61}$$

For this case, the integrands are proportional to the rate of change in the speed with respect to the time $t - r/c - \tau$. Finally, if channel is linear and the speed constant then the radiated fields are zero.

For the case of a linear filament the integrals in (54) and (55) can be evaluated in an approximate manner if certain restrictions are placed on the speed of the charges. Letting $\hat{\ell}$ be a constant vector along the direction of propagation, then the velocity appearing in the integrals of (54) and (55) can be written as

$$\mathbf{v}(u) = \hat{\ell}\, v(u) \tag{62}$$

where $u = t - r/c - \tau$. Since $\mathbf{v}'(u) = \hat{\ell}\, v'(u)$, then from (56) and (62)

$$\mathbf{h} = \hat{r} \times (\hat{r} \times \hat{\ell})\, v'(u) \tag{63}$$

Making the change of variable $w = v(u)$ and using the fact that

$$dr/d\tau = \hat{r} \cdot \mathbf{v}/p \tag{64}$$

where r is defined by (20) and (22) and p by (25), then

$$v'(u)d\tau = -p\, dw \tag{65}$$

If (63) and (65) are substituted into (54) a simpler integrand results. In general, the integral cannot be evaluated because ι and r are functions of w. If it is assumed, however, that at the bottom end point of the filament the charges are accelerated from rest to a constant velocity v_o over a distance much smaller than r_b and further that $u \approx 0$ (and therefore $\iota(\tau) \approx \iota(t - r_b/c)$) over this same distance then (54) can be written approximately as

$$\mathbf{E}_{rad}(x, t) = \frac{\hat{r}_b \times (\hat{r}_b \times \hat{\ell})}{4\pi\epsilon_o\, r_b c^2}\, \iota(t - r_b/c) \int_o^{v_o} (1 - \hat{r}_b \cdot \hat{\ell}\, w/c)^{-2}\, dw \tag{66}$$

At the top of the channel a similar contribution is made by the deceleration of charges from v_o to rest over a distance small in comparison with r_t. This contribution and (66) can be integrated to give

$$\mathbf{E}_{rad}(x, t) = \frac{v_o}{4\pi\epsilon_o c^2} \left\{ \iota(t - r_b/c)\, \hat{r}_b \times (\hat{r}_b \times \hat{\ell})/p_b r_b - \iota(t - r_t/c - t_m)\, \hat{r}_t \times (\hat{r}_t \times \hat{\ell})/p_t r_t \right\} \tag{67}$$

Similarly,

$$\mathbf{H}_{rad}(x, t) = -\frac{v_o}{4\pi c}\left\{\iota(t - r_b/c)\,\hat{r}_b \times \hat{\ell} / p_b r_b - \iota(t - r_t/c - t_m)\,\hat{r}_t \times \hat{\ell} / p_t r_t\right\} \tag{68}$$

where

$$p_b = 1 - (v_o/c)\,\hat{r}_b \cdot \hat{\ell} \tag{69}$$

$$p_t = 1 - (v_o/c)\,\hat{r}_t \cdot \hat{\ell} \tag{70}$$

and t_m is the channel length divided by v_o.

The fields given by (67) and (68) are appropriate to a current pulse, having a rectangular velocity versus time curve, which propagates along a linear filament. Results similar to these and in the latter reference identical to them, have been derived by several different approaches [Uman, 1975; Uman et al., 1978; Le Vine and Meneghini, 1978a]. The electric field signature predicted by (67) is a familiar one. For times greater than r_b/c but less than $t_m + r_t/c$, the magnitude of $\mathbf{E}_{rad}$ is proportional to the current waveform $\iota(t - r_b/c)$ with a polarization given by $\hat{r}_b \times (\hat{r}_b \times \hat{\ell})$. For times greater than $t_m + r_t/c$, each component of the field is a weighted sum of the current waveform with a time delayed and inverted image of itself. It is worth noting that as v_o approaches c and if $1 - \hat{r}_b \cdot \hat{\ell} \neq 0$, $1 - \hat{r}_t \cdot \hat{\ell} \neq 0$, then the induction terms of (33) and (34) tend to zero and previously derived expressions for the total electric and magnetic fields are recovered* [Le Vine and Meneghini, 1978a].

Equations (67) and (68) can be used to approximate the radiation fields for a current waveform traversing a piece-wise linear channel comprised of n elements of lengths $L_1, \ldots, L_n$ and directions $\ell_1, \ldots, \ell_n$, where the speed of propagation of the current waveform is

$$v(t) = v_o[U(t) - U(t - \sum_1^n L_i/v_o)]$$

and where U is the unit step function.

The electric field, for example, is simply the sum of individual terms of the form of (67) [Le Vine and Meneghini, 1978b] and can be written

*The static terms of the two solutions can be matched if the same boundary conditions are used.

$$E_{rad}(x, t) = \frac{v_o}{4\pi\epsilon_o c^2}\left\{\iota(t - r_b/c)\,\hat{r}_b \times (\hat{r}_b \times \hat{\ell}_1)/r_b p_b\right.$$

$$+ \sum_{j=1}^{n-1} \frac{\iota(t - r_j/c - T_j)}{r_j}\,\hat{r}_j \times \left[\frac{\hat{r}_j \times \hat{\ell}_{j+1}}{p(j, j+1)} - \frac{\hat{r}_j \times \hat{\ell}_j}{p(j, j)}\right]$$

$$\left. - \frac{\iota(t - r_t/c - T_j)}{r_t p_t}\,\hat{r}_t \times (\hat{r}_t \times \hat{\ell}_n)\right\} \tag{71}$$

where r_j is the distance from the jth channel transition point to the observer and

$$T_j = \sum_{k=1}^{j} L_k/v_o \tag{72}$$

$$p(i, j) = 1 - (v_o/c)\,(\hat{r}_i \cdot \hat{\ell}_j) \tag{73}$$

Note that r_t is the distance from the top of the nth channel segment to the observer, while r_b is the distance from the bottom of the first segment to the observer.

Terms in the summation of (71) correspond to radiation arising from the channel transition points. It is not obvious that these contributions are identical to the limiting form that would be obtained from (54). By "limiting form" we mean the field produced under conditions of a current pulse of constant speed and a channel geometry in which the curvature is non-zero only near isolated transition points. Unfortunately, we have not been able to carry out the integration of (54) in this limit. Numerical comparisons between (54) and (71) are discussed in a subsequent section of this paper.

Channel Geometries

a) Channel tortuosity: hyperbolic channel

One of the simplest continuous and differentiable channel models that can be used to study the effects of curvature is the hyperbola. In addition to its analytic simplicity, it also lends itself to a comparison of a two element piece-wise linear channel model if the elements are chosen to coincide with the asymptotes of the hyperbola. In fact, if the equations for the asymptotes are given then there exists a family of hyperbolas having these asymptotes which includes the degenerate case

of the piece-wise linear channel, i.e. the asymptotes themselves. Since the curvature of the channel is the change in angle with respect to arc length, the integrated curvature of any hyperbola depends only on the angle subtended by the asymptotes*. This property provides a convenient way to quantify the effects of curvature on the radiated field.

Assuming that the hyperbola lies in the x-z plane with the transverse axis along the x axis and with a origin displaced along the vertical (z) direction, then

$$\frac{x^2}{a^2} - \frac{(z-d)^2}{b^2} = 1 \tag{74}$$

In the subsequent discussion and in the numerical results, we choose the $0 \leq z \leq 2d$ segment of branch of the hyperbola for which $x \geq 0$.

The square of the speed, v, of a charged particle moving along the hyperbola is

$$v^2(t) = (dx/dt)^2 + (dz/dt)^2 \tag{75}$$

To find the trajectory of the charges (or, equivalently, the trajectory of the current waveform) as a function of time, (74) is differentiated with respect to t. Squaring the result and using (74) and (75) to eliminate x^2 and $(dx/dt)^2$ gives

$$\left(\frac{(z-d)^2 + \gamma^2}{(z-d)^2 + b^2}\right)^{1/2} dz = \frac{bv(t)}{(a^2+b^2)^{1/2}}\, dt \tag{76}$$

where

$$\gamma = b^2/(a^2+b^2)^{1/2} \tag{77}$$

Integrating (76) from z(0) to z(t) yields [Gradshteyn and Ryzhik, 1965]

$$v_o^{-1}\int_o^t v(t)dt = t_o + c_1\, \mathrm{sgn}\,(z-d)\left\{\frac{\gamma^2}{b} F(\beta_1, q) - b\, E(\beta_1, q) + |z-d|\left(\frac{b^2+(z-d)^2}{\gamma^2+(z-d)^2}\right)^{1/2}\right\} \tag{78}$$

*Since the channel model uses only a finite portion of the hyperbola, this statement is not strictly correct. For the parameters used in the numerical calculations, however, it is a good approximation.

where F, E are elliptic integrals of the first and second kind, respectively,

$$F(\phi, k) = \int_0^{\phi} (1 - k^2 \sin^2 x)^{-1/2} \, dx \tag{79}$$

$$E(\phi, k) = \int_0^{\phi} (1 - k^2 \sin^2 x)^{1/2} \, dx \tag{80}$$

The constant time, t_o, is given by

$$t_o = c_1 \left(\frac{\gamma^2}{b} \, F(\beta_2, q) - b \, E(\beta_2, q) + d \left(\frac{b^2 + d^2}{\gamma^2 + d^2} \right)^{1/2} \right) \tag{81}$$

with

$$c_1 = (a^2 + b^2)^{1/2} / v_o b \tag{82}$$

$$q = a/(a^2 + b^2)^{1/2} \tag{83}$$

$$\beta_1 = \mathrm{Tan}^{-1}(|d - z| / b) \tag{84}$$

$$\beta_2 = \mathrm{Tan}^{-1}(d/b) \tag{85}$$

and

$$\mathrm{sgn}(x) = \begin{cases} 1 & x > 0 \\ -1 & x < 0 \end{cases} \tag{86}$$

The constant v_o , defined below, has dimensions of velocity.

To complete the specification of charge motion along the channel, the speed and acceleration are assigned so that they are zero at the channel end points and continuous everywhere. Choosing the speed to be a cubic polynomial in t both for $0 \leq t \leq t_1$ and $t_2 \leq t \leq t_m$ and an exponential for $t_1 \leq t \leq t_2$ provides a sufficient number of constants to satisfy these requirements. Note that t_m is the time taken for a charge to transverse the entire channel. One reason for choosing this particular model is that it allows us to obtain approximations to the velocity versus time curves computed by Leise and Taylor (1977).

The result is

$$v(t) = \begin{cases} v_o(t/t_1)^2 (a_1 + a_2(t/t_1)) & 0 \leq t \leq t_1 \\ v_o\, e^{-\beta(t - t_1)} & t_1 \leq t \leq t_2 \\ v_o((t - t_m)/t_f)^2 (a_3 + a_4(t - t_m)/t_f)\, e^{-\beta(t_2 - t_1)} & t_2 \leq t \leq t_m \end{cases} \quad (87)$$

where $v_o = v(t_1)$ is the maximum speed and

$$t_f = t_m - t_2 \quad (88)$$

$$a_1 = 3 + \beta t_1 \; ; \; a_2 = -2 - \beta t_1 \quad (89)$$

$$a_3 = 3 - \beta t_f \; ; \; a_4 = 2 - \beta t_f \quad (90)$$

Expressions for the z components of the velocity and acceleration can now be found from (76) and (87)

$$v_z = dz/dt = \frac{bv(t)}{(a^2 + b^2)^{1/2}} \left(\frac{(z - d)^2 + b^2}{(z - d)^2 + \gamma^2} \right)^{1/2} \quad (91)$$

$$v'_z = d^2z/dt^2 = \frac{v'(t)v_z}{v(t)} + \frac{(bv(t))^2 \; (z - d)\,(\gamma^2 - b^2)}{(a^2 + b^2)\; ((z - d)^2 + \gamma^2)^2} \quad (92)$$

where $v'(t)$ is determined by differentiating (87). Equations for x, v_x, v'_x are derived from (74) and (75) by a similar procedure. Since x is more conveniently computed from (76), the results are given here only for v_x, v'_x which are

$$v_x = \frac{a\, v\,(t)}{(a^2 + b^2)^{1/2}} \left(\frac{x^2 - a^2}{x^2 - \sigma^2} \right)^{1/2} \text{sgn}\,(z - d) \quad (93)$$

$$v'_x = \frac{v'(t)v_x}{v(t)} + \frac{(a\, v(t))^2 \; (a^2 - \sigma^2)x}{(a^2 + b^2) \; (x^2 - \sigma^2)^2} \quad (94)$$

with

$$\sigma = a^2/(a^2 + b^2)^{1/2} \quad (95)$$

The foregoing equations can now be used in (33) and (34) to generate the fields for arbitrary observation points and times. Since the evaluation of the integrals is somewhat complicated and since simplifications are possible, it is worth indicating how the calculations are made.

To find z as a function of t, equally spaced values of z are taken from 0 to 2d and the corresponding value of t is obtained from (78). To express z in terms of equally spaced time intervals, a linear interpolation is performed. The x(t) value is then found from (74) with $x \geq 0$. Once x(t) and z(t) are known, the velocity and acceleration are computed from equations (87) and (91) through (94). These quantities then determine f(t), f'(t), f''(t).

As indicated earlier, for each sample point τ in the numerical integration of (33) and (34), r can be found from the equations

$$r = |x - x'| \tag{20}$$

with

$$x' = f(t - |x - x'|/c - \tau) \tag{22}$$

An easier way to evaluate r is possible, however. Letting

$$x' = f(T) \tag{96}$$

then (22) can be written

$$f(T) = f(t - |x - f(T)|/c - \tau) \tag{97}$$

The function f is assumed to be one to one so that the arguments of f can be equated:

$$T = t - |x - f(T)|/c - \tau \tag{98}$$

Since t, x and f are known and τ is fixed, (98) can be solved numerically for T. From T, x' is found from (96) which determines, in turn, r, v and v'.

b) Linear Channel Model

For the case of a linear channel, the specification of f(t), f'(t) and f''(t) is straightforward. Letting $(x_1, 0, z_1)$, $(x_2, 0, z_2)$ be the bottom and top end points of the channel then the equation

for any point (x, 0, z) on the channel is

$$z - z_1 = s(x - x_1) \tag{99}$$

where

$$s = (z_2 - z_1)/(x_2 - x_1)\,; \quad x_2 \neq x_1 \tag{100}$$

Solving for x and z as a function of the time t yields

$$x(t) = x_1 + (1 + s^2)^{-1/2} \int_o^t v(t)\, dt \tag{101}$$

$$z(t) = z_1 + s(1 + s^2)^{-1/2} \int_o^t v(t)\, dt \tag{102}$$

These equations determine $f(t) = (x(t), 0, z(t))$; $f'(t)$ and $f''(t)$ are then obtained by successive differentiations. Note that if $x_1 = x_2$, z(t) can be obtained from (102) by letting $s \to \infty$. As in the hyperbolic channel, the speed v(t) is assumed to be given by (87).

Numerical Examples

The cases presented illustrate some of the characteristics of the field solutions given by (33) and (34). In all examples, the observer is located on the surface of a perfectly conducting plane; thus, only the normal electric field and tangential magnetic field are non-zero. The current waveform is assumed to be

$$\iota(\tau) = 30{,}000\,(e^{-.04\tau} - e^{-2\tau}) \tag{103}$$

where τ is expressed in microseconds and $\iota(\tau)$ in amperes. In all figures the quantities v_o, t_1 and t_f in (87), (88) are taken such that $v_o = c/3$ and $t_1 = t_f$. Each curve consists of 400 equally spaced samples in the time domain. The CPU time required for a representative curve is approximately 40 s on an IBM 3081.

To show the effects of changes in speed independent of the channel curvature, a linear channel model is used. Examples are shown in figures 1 and 2. For both figures the channel is vertical

with bottom and top end points at $x = y = z = 0$ and $x = y = 0$, $z = 4$ km, respectively. The observer is located at $x = 100$ km, and $y = z = 0$. In figure 1 the curves A, B, C correspond to values of t_1, as defined in (87), equal to 16, 8, 2 μs respectively. In all cases $\beta = 0$. Curve D was generated by means of (67); all others from (33). As mentioned earlier, curve D represents the field in the limiting case $t_1 \to 0$ and is proportional to a sum of two current waveforms where one is displaced in time and inverted with respect to the other. Increasing t_1 has two effects: the curves are 'stretched' and the peak amplitude of the field is reduced such that the time integral of the magnitude of the field remains approximately constant. It should be noted that in the case of a linear filament (67) has been shown to approximate (33) well as long as t_1 is less than about 1 μs. This remains true for different channel orientations and propagation speeds, v_o.

In figure 1 the parameter β as defined in (87) equals zero. In figure 2, t_1 is fixed at 4 μs while β is varied. The curves A, B and C correspond to values of β equal to 2×10^4, 1.5×10^4 and 10^4 s^{-1}, respectively. The speed versus time curves for these cases are shown in the inset. Since t_1 and the maximum velocity, v_o, are constant, the peak field occurs at approximately 4 μs in all cases.

Increasing β tends to narrow the width of the waveform and to decrease the positive overshoot. This latter effect is caused by a decrease in acceleration near the channel top; for example, at $\beta = 10^4$ s^{-1} the charges must be decelerated from $v = 6.3 \times 10^7$ ms^{-1} to zero within 4 μs while for $\beta = 2 \times 10^4$ s^{-1} they are decelerated from the smaller value $v = 2.5 \times 10^7$ ms^{-1} to zero within the same time span.

To explain the narrowing of the initial portion of the field, note that for $\beta = 0$, charge acceleration at the channel bottom produces a negative z directed field. For $\beta \neq 0$, the charges, having reached their maximum velocity, are then decelerated, i.e., $v'(t) = -\beta e^{-\beta t}$, which results in a positively directed E_z. The total field, therefore, is the sum of negative and positive z components, the latter contribution beginning 4 μs after the first. The result is that the width of the negative portion of the waveform narrows as β increases. It should be noted that the field signatures given by curves A and B are qualitatively similar to the radiated waveform proposed by Leise and Taylor (1977). This is not surprising since we have essentially proceeded in a reverse direction by starting with a velocity curve qualitatively similar to their derived curve and then using this to compute the field.

To study the effects of tortuosity on the fields, the speed of the current waveform is chosen to be a constant, v_o, in figures 3 and 4; i.e., $t_1 = 0$, $t_f = 0$ and $\beta = 0$ in (87). This situation is not the

same as obtained by taking the limit $t_1 = t_f \rightarrow 0$ which yields radiation fields of the form given by (67). Rather, the assumption is simply used to eliminate the sources of radiation from the ends of the filament and isolate curvature effects.

In figure 3 are shown three curves of the z component of the electric field for an observer at $x = 100$ km, $y = z = 0$. The channel geometry is a hyperbola, given by (76), with $x > 0$, $0 \leq z \leq 3$ km ($d = 1.5$ km) and $a = b$. Curves A, B and C correspond to values of 'a' equal to 500, 100, and 20 m, respectively. The channel geometries are shown in the inset. Since the ratio b/a is constant the asymptotes of the channels are identical and therefore the total integrated curvature of each of the channels is approximately constant. As 'a' decreases the field is seen to tend toward zero for times less than 25 μs After 25 μs the shape of the curve C corresponding to $a = 20$ m is similar to the current waveform. This behavior can be qualitatively explained by noting that as 'a' decreases, the only portion of the channel where significant charge acceleration occurs is near the 'bend', i.e., the apex of the hyperbola. In the limit of small 'a' the radiation field, (which is the dominant contributor to the total field at this distance), originates entirely from this point and is proportional to the current waveform, i. Several examples were run for 'a' less than 20 m, down to a minimum of 2 m. The corresponding field change, however, is small.

Figure 4 shows the effect of changing the slope of the asymptotes. The channel geometry is again given by (74) with $x > 0$, $0 \leq z \leq 3$ km but now with $a = 2b$. Curves A, B, and C correspond to values of 'a' equal to 500, 100, and 20 m. Notice that amplitudes of the field are increased as compared to those of figure 3. This is reasonable in the sense that the integrated curvature of the channel has increased over that assumed in figure 3. Since the integrand of (54) is proportional to curvature for the $v = v_0$ case then, in general, larger fields can be expected.

The combined effects of channel curvature and linear acceleration on the electric and magnetic fields are shown in figures 5 and 6. For both figures the channel geometry is hyperbolic with $x > 0$, $0 \leq z \leq 3$ km and $a = b = 100$ m. The velocity is again given by (87) with $\beta = 0$ and $t_1 = 2$ μs. Curves A, B and C correspond to observer distances of 1 km, 10 km and 100 km along the x-axis. For curves A and B in figure 5, the static contribution is evident. This is a consequence of the simple charge transport model used and represents the accumulation of charge at the top end of the channel. Since the bottom of the channel is on perfectly conducting plane, the static contribution from this endpoint is zero. For the magnetic field, plotted in figure 6, the static contribution is, as shown by (34), zero.

A number of numerical comparisons were made between the fields predicted by the piece-wise linear representation of (71) and the Lienard-Wiechert solution of (33). The comparisons were made in the far field and therefore (33) and (54) are essentially the same. To make the geometries as close as possible n, in (71), was set equal to 2 and for (33) a hyperbolic channel was chosen with parameters 'a' and 'b' as small as possible without incurring sampling errors. In addition $t_1 = t_f$ in (87) was chosen to be small to approximate the delta function acceleration at the end points inherent in (67) and (71). As indicated earlier, the radiation arising from the end points of the channel are in good agreement for the cases considered. On the other hand, the fields arising from the channel transition points showed differences which generally increase with increasing channel curvature. For example, when the curvature is small, 2a = b, the two solutions are in good agreement. At a = 2b, however, the ratio of the Lienard-Wiechert to the piece-wise linear solution is approximately two for v_o between c/10 and c/1.25. As noted before, we have been unable to analytically evaluate (54) in the limiting case of a piece-wise linear channel. Some qualitative understanding of the differences between (54) and (71) can be gained, however, by noting that in deriving (71) the velocity and acceleration were assumed to be colinear and therefore the term $\mathbf{h}_1 = \hat{r} \times (v/c \times v')$ in the integrand of (54) was zero. On the other hand, as we let the parameters 'a' and 'b' in the equation for the hyperbola approach zero, the geometry will tend toward a piece-wise linear channel. In general, however, $\mathbf{h}_1$ will be non-zero and therefore will contribute to the Lienard-Wiechert solution.

Discussion and Conclusions

A form of the Lienard-Wiechert solution has been used to determine the electric and magnetic fields associated with a commonly used lightning return stroke model. An apparent advantage of this form of solution is that parameters of the current waveform can be assigned independently of the channel geometry. Because of this, a class of geometries can be studied in the context of the same return stroke model. For example, one type of geometry that can be analyzed is a cubic spline approximation to photographed lightning channels.

Effects of linear acceleration and curvature were studied by means of two simple channel geometries: the linear and the hyperbolic. For the special case of a linear filament and a rectangular velocity versus time profile, the solution is in good agreement with previous work. Significant changes in the signature appear, however, when the shape of the velocity profile is altered.

In the case of the hyperbolic filament, the radiated fields are functions of the curvature, observer location and current waveform shape. Only in cases where the non-zero curvature is concentrated about a small segment of the channel do the signatures approximate the current waveform shape. Preliminary numerical results also have shown that if the velocity profile of the current waveform is rectangular and the non-zero curvature occurs only near isolated points along the channel, then the Lienard-Wiechert and the piece-wise linear representations are in fair agreement in many cases. In particular, the two solutions give nearly identical results for the radiation arising from the channel end points. As to the radiation from the channel transition points, discrepancies between the two solutions are observed that become more pronounced with increasing channel curvature. One of the reasons for the differences appears to be the assumption used in deriving the piece-wise linear solution: that the velocity and acceleration are colinear.

It should be mentioned in conclusion that several other issues pertaining to the Lienard-Wiechert representation have not been answered: whether the field given by (33) is equivalent to the Panofsky and Phillips solution as applied to the return stroke model by Leise and Taylor (1977); and whether a form of the Lienard-Wiechert representation can be derived for more complicated models of the return stroke [Price and Pierce, 1977; Lin et al., 1980].

APPENDIX – CALCULATION OF THE FIELDS

The electric **E** and magnetic **H** fields are given by

$$\mathbf{E} = -\nabla\phi - \partial\mathbf{A}/\partial t \tag{A1}$$

$$\mathbf{H} = \frac{1}{\mu_0}\nabla\times\mathbf{A} \tag{A2}$$

where ϕ and **A** are, from (15) and (16),

$$4\pi\epsilon_0\phi = \int_\tau \int_{t'} \frac{\iota(\tau)\,\delta(t' - (t - r/c))}{r}\,dt'\,d\tau \tag{A3}$$

$$4\pi\epsilon_0 c^2\mathbf{A} = \int_\tau \int_{t'} \frac{\iota(\tau)\;\mathbf{f}'(t'-\tau)\,\delta(t' - (t - r/c))\,dt'\,d\tau}{r} \tag{A4}$$

with

$$r = |\mathbf{x} - \mathbf{f}(t' - \tau)| \tag{A5}$$

The limits of integration on t' and τ are $(-\infty, \infty)$.

Taking the gradient of (A3) and interchanging the order of integration and differentiation yields

$$4\pi\epsilon_0\nabla\phi = \int_\tau \iota(\tau)\,(\mathbf{I}_A(\tau) + \mathbf{I}_B(\tau))\,d\tau \tag{A6}$$

where

$$\mathbf{I}_A(\tau) = -\int_{t'} \frac{\hat{\mathbf{r}}}{r^2}\,\delta(t' - (t - r/c))\,dt' \tag{A7}$$

$$\mathbf{I}_B(\tau) = \int_{t'} \frac{1}{r}\,\nabla\delta(t' - (t - r/c))\,dt' \tag{A8}$$

By an application of the chain rule $\nabla\delta(t' - (t - r/c))$ can be written as

$\hat{r}\,\delta'(t' - (t - r/c))/c$ where the prime on the delta function denotes differentiation with respect to its argument.

Following Jackson (1962), the change of variable $w = t' + r/c$ is made in (A7) and (A8). From (A5) we find that

$$dw/dt' = 1 - v \cdot \hat{r}/c \equiv p \tag{A9}$$

with

$$v = f'(t' - \tau) \tag{A10}$$

Equations (A7) and (A8) become

$$I_A(\tau) = -\int \frac{\hat{r}\,\delta(w - t)}{pr^2}\, dw \tag{A11}$$

$$I_B(\tau) = \int \frac{\hat{r}\,\delta'(w - t)}{prc}\, dw \tag{A12}$$

$I_A(t)$ can be integrated immediately to give

$$I_A(\tau) = -(\hat{r}/pr^2)_o \tag{A13}$$

where the subscript o means that all variables within the brackets are to be evaluated at $t' = t - r/c$. Explicitly,

$$r = |x - x'| \tag{A14}$$

$$p = 1 - v \cdot \hat{r}/c \tag{A15}$$

with

$$x' = f(t - |x - x'|/c - \tau) \tag{A16}$$

$$v = f'(t - |x - x'|/c - \tau) \tag{A17}$$

Integrating (A12) by parts gives

$$I_B(\tau) = \left\{\frac{d}{dw}\left(\frac{\hat{r}}{prc}\right)\right\}_o \tag{A18}$$

Using the facts that

$$\frac{d}{dw}\left(\frac{\hat{r}}{pr}\right) = p^{-1}\frac{d}{dt'}\left(\frac{\hat{r}}{pr}\right) \tag{A19}$$

$$\frac{d}{dt'}(pr)^{-1} = -(pr)^{-2}\left(\frac{v^2}{c} - v\cdot\hat{r} - \frac{r\hat{r}\cdot v'}{c}\right) \tag{A20}$$

$$\frac{d\hat{r}}{dt'} = -r^{-1}(v - \hat{r}(v\cdot\hat{r})) \tag{A21}$$

then

$$I_B(\tau) = \left\{\frac{1}{p^3r^2c}\left[\hat{r}(v^2/c - v\cdot\hat{r} - r\hat{r}\cdot v'/c) + (v - \hat{r}(v\cdot\hat{r}))p\right]\right\}_o \tag{A22}$$

From (A6), (A14) and (A22),

$$4\pi\epsilon_o\nabla\phi = \int_\tau \iota(\tau)\left\{\frac{1}{p^3r^2c}\left[\hat{r}(v^2/c - v\cdot\hat{r} - r\hat{r}\cdot v'/c) + p(v - \hat{r}(v\cdot\hat{r}))\right]\right\}_o d\tau \tag{A23}$$

The calculation of $\partial A/\partial t$ follows closely that for $\nabla\phi$. The result is

$$4\pi\epsilon_o c^2\,\partial A/\partial t = \int \iota(\tau)\left\{\frac{1}{p^3r^2}\left[prv' - vv^2/c - v\cdot\hat{r} - r\hat{r}\cdot v'/c\right]\right\}_o d\tau \tag{A24}$$

Inserting $\nabla\phi$ into $\partial A/\partial t$ into (A1) and using the identities

$$\hat{r}\times\left[(r - v/c)\times v'\right] = \hat{r}\cdot v'(\hat{r} - v/c) - v'p \tag{A25}$$

$$(\hat{r} - v/c)(1 - (v/c)^2) = \hat{r}p^2 - p(v - \hat{r}(v\cdot\hat{r}))/c - (v^2/c - v\cdot\hat{r})(\hat{r} - v/c)/c \tag{A26}$$

then

$$E(x, t) = \frac{1}{4\pi e_o} \int \iota(\tau)\,(F_1 + F_2)d\tau \tag{A27}$$

where

$$F_1 = \left\{ \frac{1}{p^3 r^2} (\hat{r} - v/c)\,(1 - (v/c)^2 \right\}_o \tag{A28}$$

$$F_2 = \left\{ \frac{1}{p^3 c^2 r} \hat{r} \times [(\hat{r} - v/c) \times v'] \right\}_o \tag{A29}$$

To obtain the magnetic field, the curl of (A4) is taken which gives

$$4\pi e_o c^2 \ \nabla \times A(x, t) = -\int \iota(\tau)\,(I_c(\tau) - I_d(\tau))\,d\tau \tag{A30}$$

where

$$I_c(\tau) = \int \frac{f'(t' - \tau) \times \hat{r}}{rc} \ \delta'(t' - (t - r/c))\,dt' \tag{A31}$$

$$I_d(\tau) = \int \frac{f'(t' - \tau) \times \hat{r}}{r^2} \ \delta(t' - (t - r/c))dt' \tag{A32}$$

Proceeding as before and using (A2) and the identities

$$-\hat{r} \times \left\{ \hat{r} \times [(\hat{r} - v/c) \times v'] \right\} = \hat{r} \times \left\{ (\hat{r} \cdot v')v/c + pv' \right\} \tag{A33}$$

$$-c^3 \hat{r} \times [(\hat{r} - v/c)\,(1 - v^2/c^2)] = (v \times \hat{r})\,(v^2 - c^2) \tag{A34}$$

then

$$H(x, t) = \frac{c}{4\pi} \int \iota(\tau) \left\{ \hat{r} \times (F_1 + F_2) \right\}_o d\tau \tag{A35}$$

To simplify the notation in the text the subscripts o have been omitted.

REFERENCES

Gradshteyn, I.S. and I. M. Ryzhik (1965), Table of Integrals, Series and Products, 4th edition, 1086 pp., Academic Press, New York.

Hay, G. E. (1953), Vector and Tensor Analysis, 193 pp., Dover, New York.

Hill, R. D. (1968), Analysis of irregular paths of lightning channels, J. Geophys. Res., 73, pp. 1897-1906.

Hill, R. D. (1969), Electromagnetic radiation from erratic paths of lightning strokes, J. Geophys. Res. 74, pp. 1922-1929.

Jackson, J. D. (1962), Classical Electrodynamics, 1st edition, 641 pp., John Wiley and Sons, Inc., New York.

Jones, D. S. (1964), The Theory of Electromagnetism, 807 pp., Pergamon Press, Oxford.

Leise, J. A. and W. L. Taylor (1977), A transmission line model with general velocities for lightning, J. Geophys. Res., 82, pp. 391-396.

Le Vine, D. M. and R. Meneghini (1978a), Electromagnetic fields radiated from a lightning return stroke: application of an exact solution to Maxwell's equations, J. Geophys. Res., 83, pp. 2377-2384.

Le Vine, D. M. and R. Meneghini (1978b), Simulation of radiation from lightning return strokes, Radio Science, 6, pp. 801-809.

Lin, Y. T., M. A. Uman and R. B. Standler (1980) Lightning return stroke models, J. Geophys. Res., 85, 1571-1583.

Marney, G. O. and K. Shanmugam (1971), Effect of channel orientation on the frequency spectrum of lightning discharges, J. Geophys. Res., 76, 4198-4202.

McLain D. K. and M. A. Uman (1971), Exact expression and moment approximation for the electric field intensity of the lightning return stroke, J. Geophys. Res., 76, 2101-2105.

Panofsky, W. K. H. and M. Phillips (1962), Classical Electricity and Magnetism, 494 pp., Addison-Wesley, Reading, Mass.

Price, G. H. and E. T. Pierce (1977), The modeling of channel current in the lightning return stroke, Radio Science, 12, 381-388.

Stoker, J. J., (1969), Differential Geometry, 404 pp., Wiley-Interscience, New York.

Uman, M. A., D. K. McLain and E. P. Krider (1975), The electromagnetic radiation from a finite antenna, Am. J. Phys., 43, pp. 33-38.

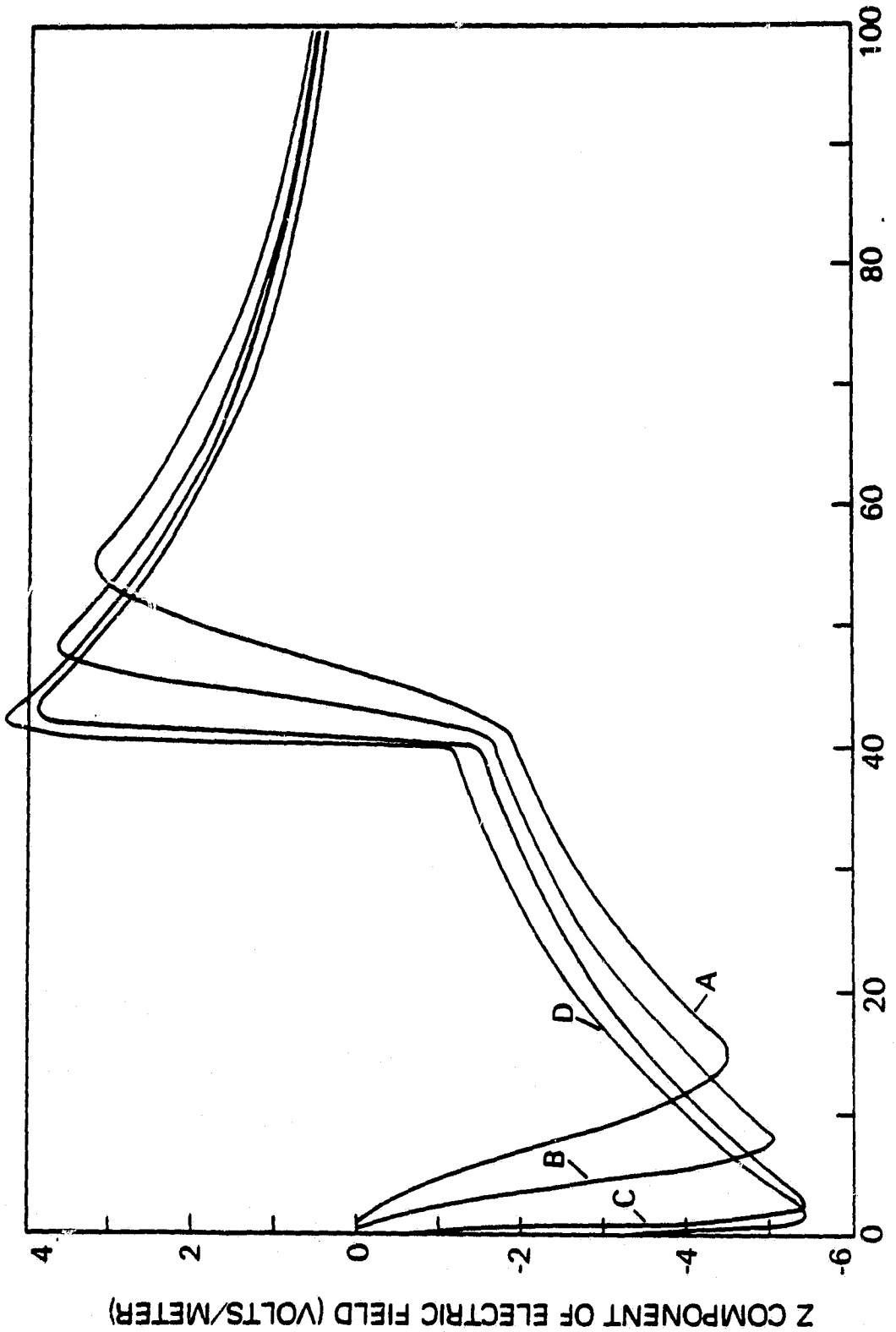

Figure 1. z component of electric field versus time for a 4 km vertical filament and an observer along the x-axis at 100 km. Curves A, B, C, and D correspond to $t_J = 16, 8, 2$, and $t_J \rightarrow 0$ μs, respectively.

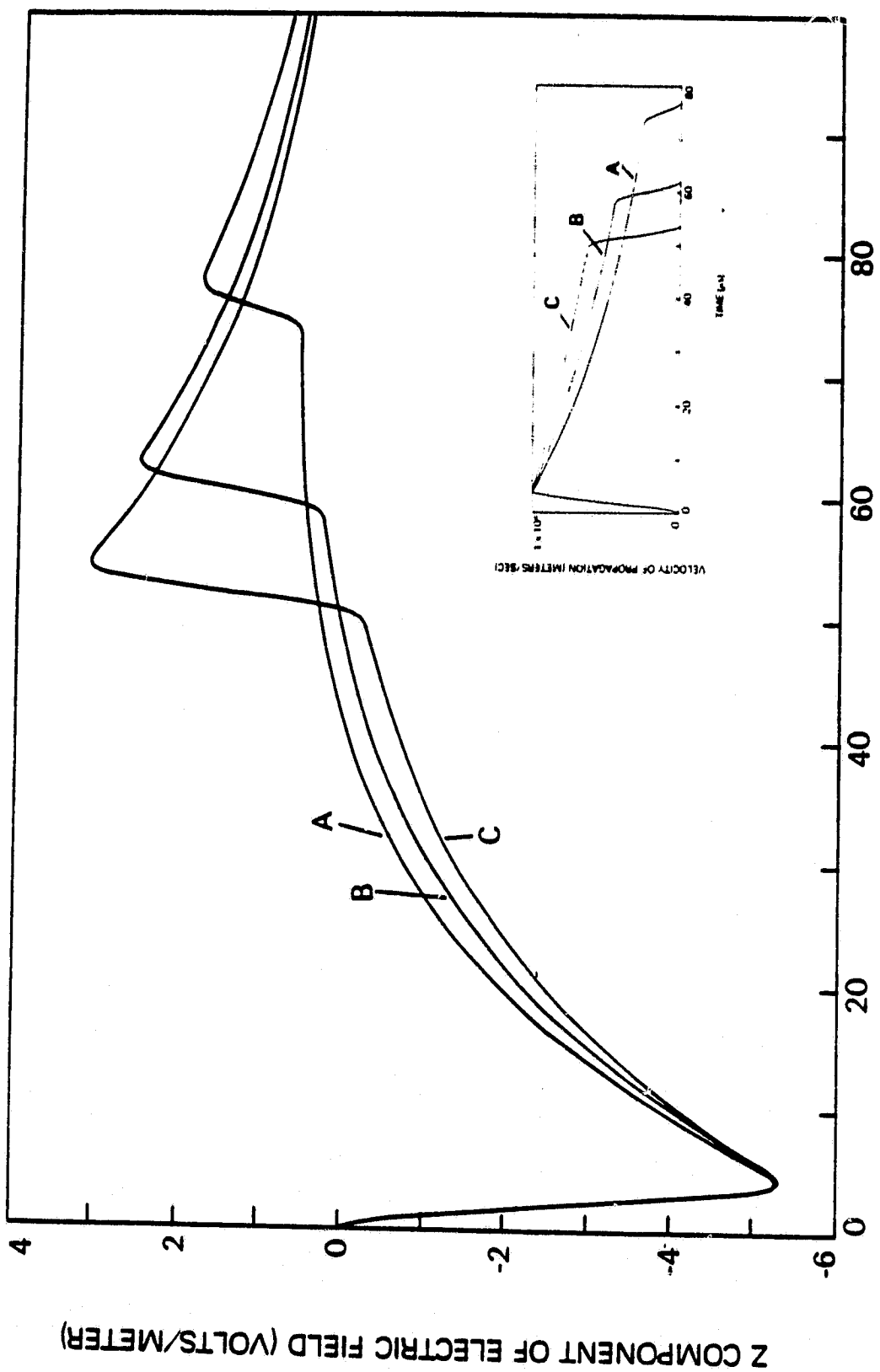

Figure 2. Same channel and observer as in figure 1. $t_1 = 4\ \mu s$. Curves A, B, and C correspond to values of $\beta = 2 \times 10^4$, 1.5×10^4 and $10^4\ s^{-1}$, respectively. The inset shows the corresponding curves of the current waveform velocity versus time.

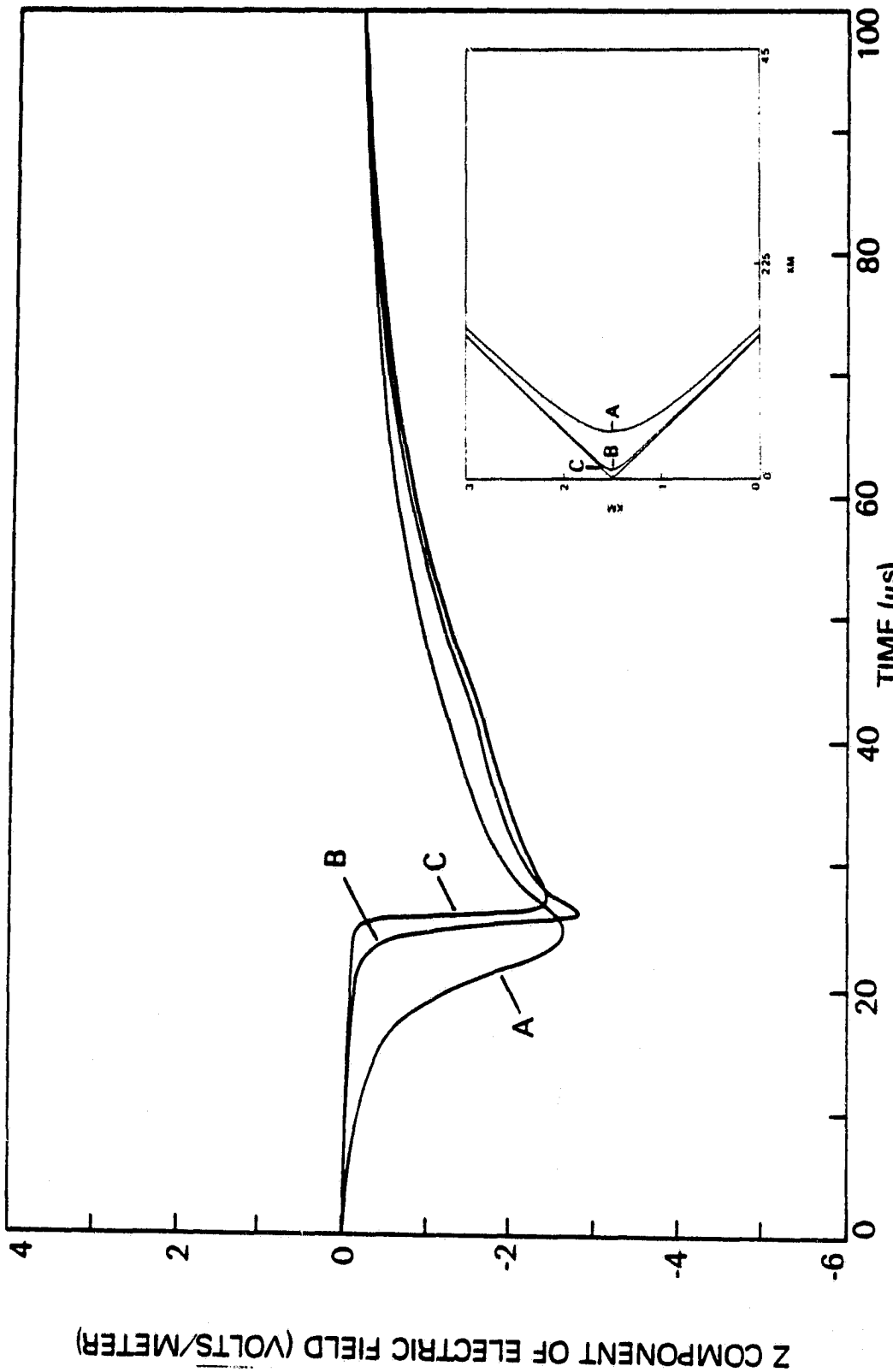

Figure 3. z component of electric field versus time for hyperbolic channel geometries. The observer is located along the x-axis, 100 km distant, $t_1 = 0$ μs. Curves A, B, C, correspond to values of a = 500, 100 and 20 m, respectively, where a = b. The associated channel geometries are shown in the inset.

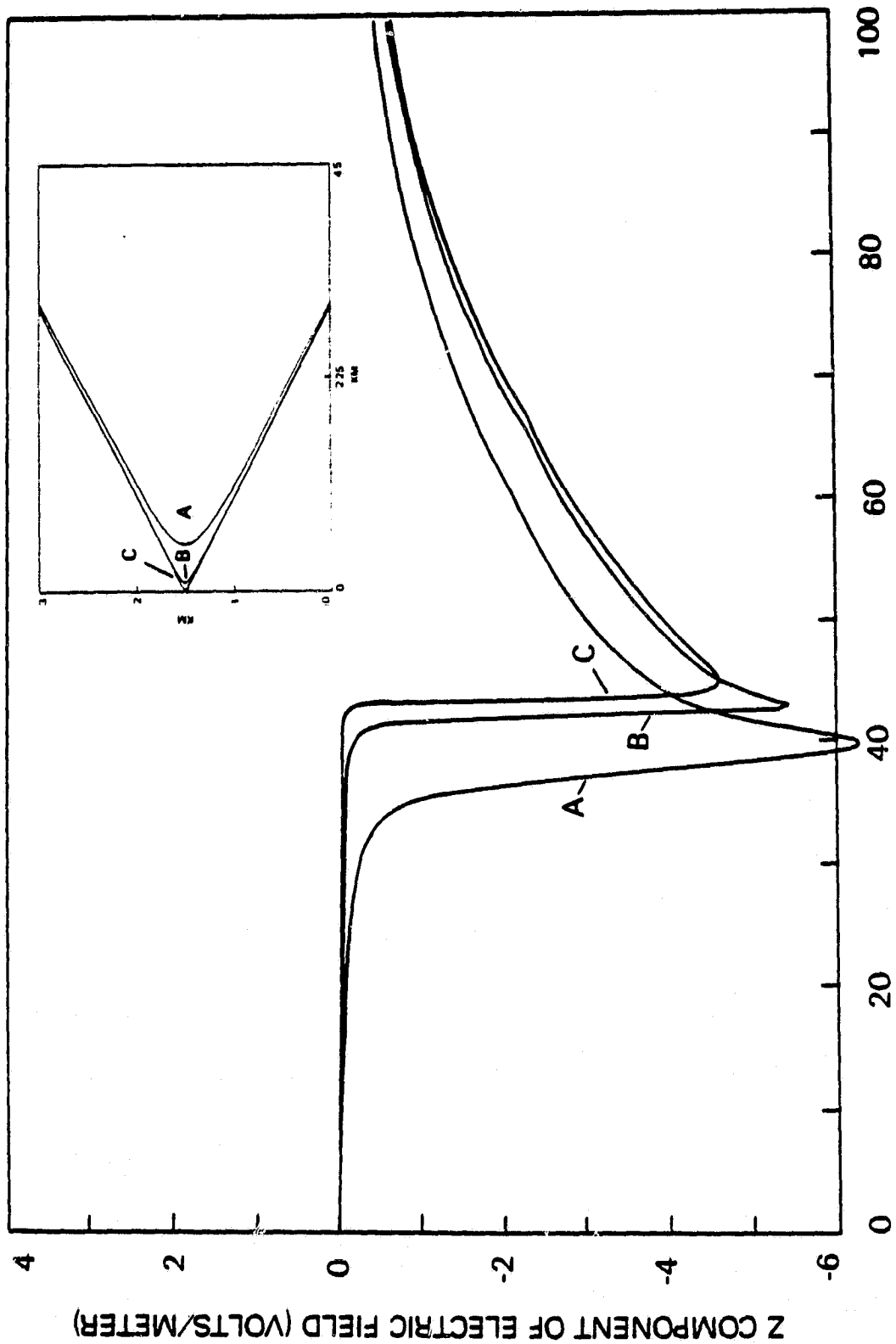

Figure 4. Same as figure 3 except that a = 2b.

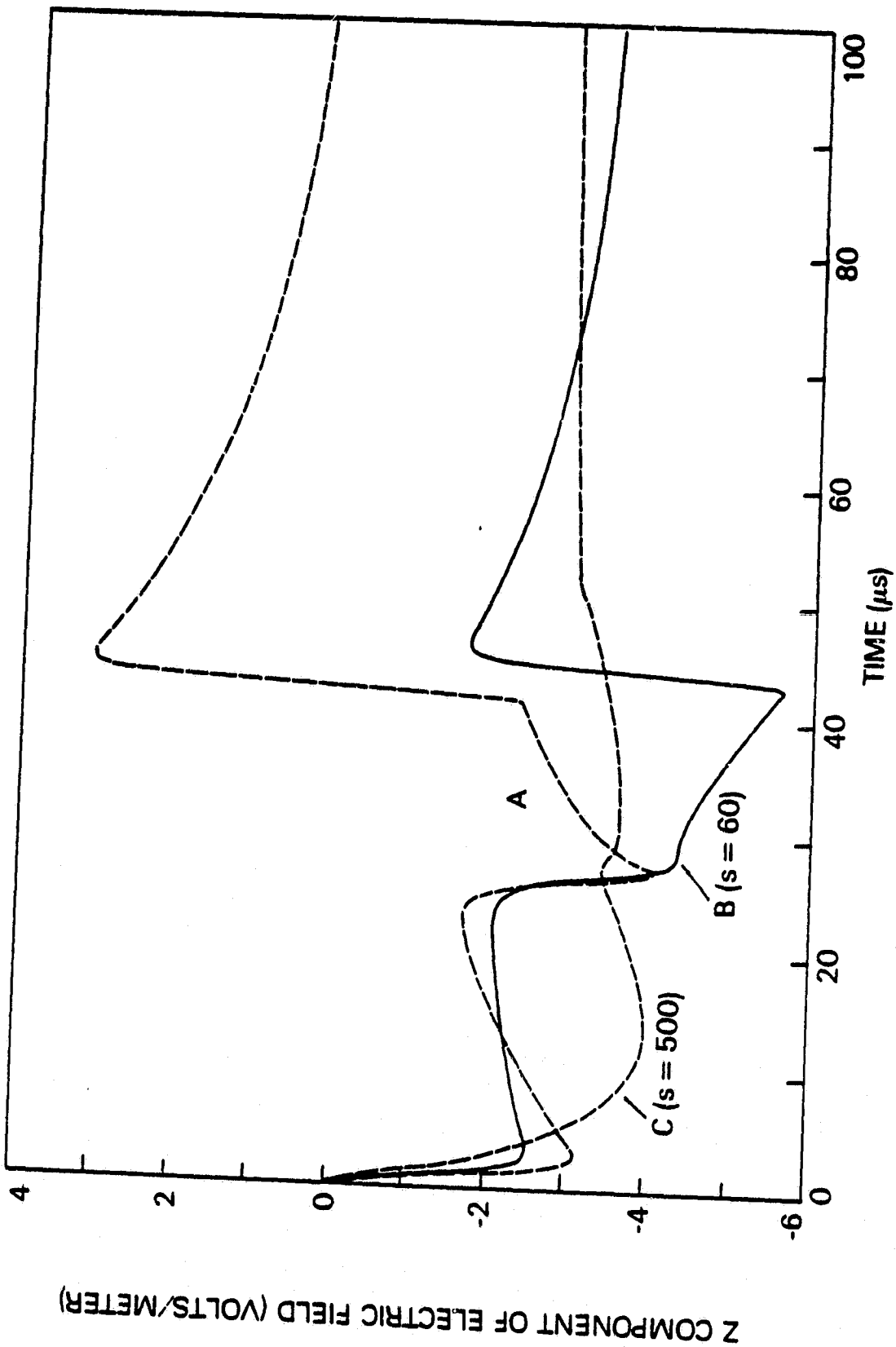

Figure 5. z component of electric field versus time for a hyperbolic channel with a = b = 100 m, t_1 = 2 μs. Curves A, B, and C correspond to observation distances along the x-axis equal to 100 km, 10 km and 2 km, respectively. The scales for curves B and C are obtained by multiplying the numbers along the ordinate by the scale factor s.

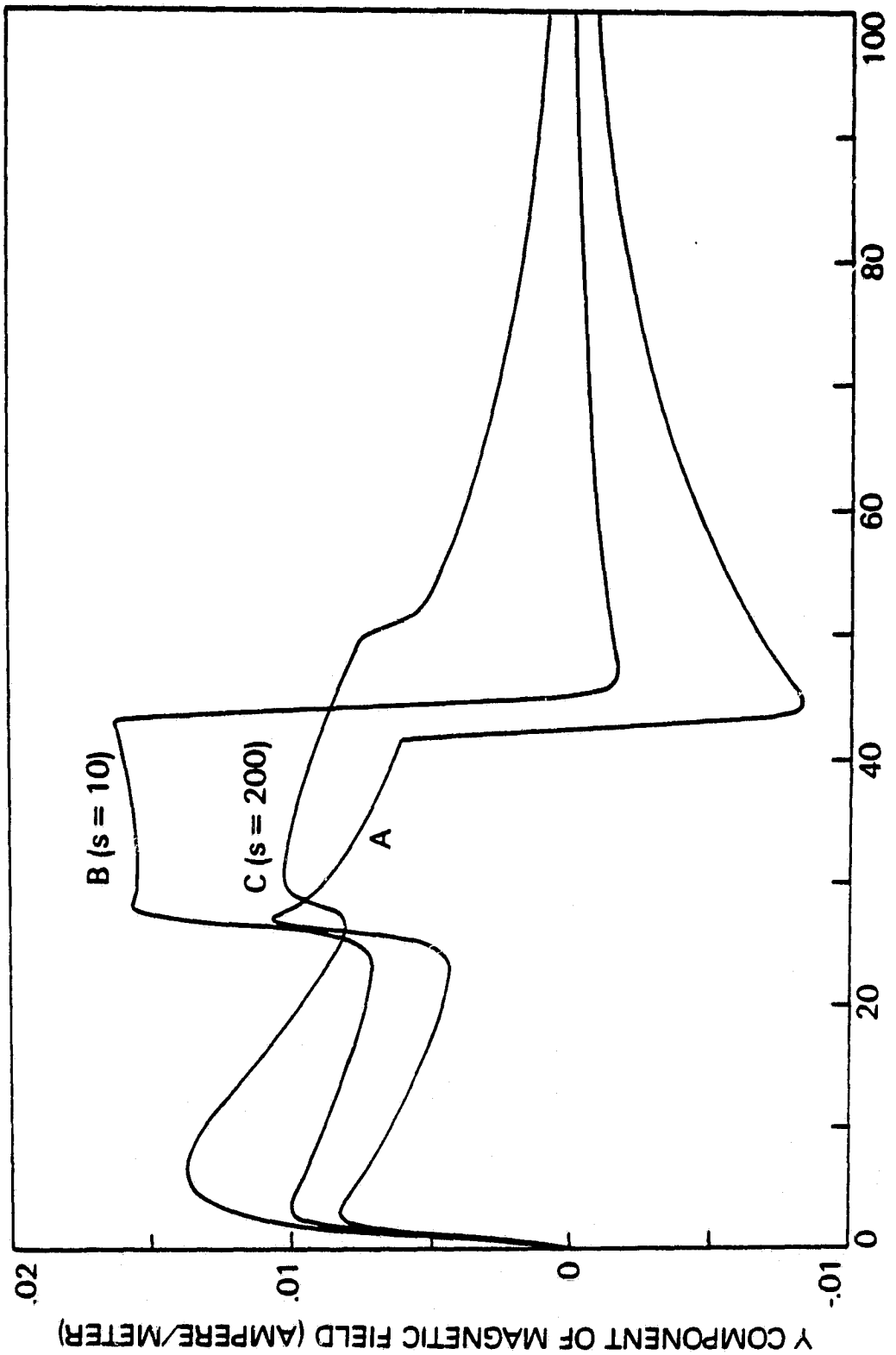

Figure 6. y component of the magnetic field versus time. Channel parameters and observation distances are the same as in figure 5.